Int J Thermophys (2009) 30:1270–1282
DOI 10.1007/s10765-009-0560-z

Thermal-Diffusivity Measurement of Ceramic Coatings at High Temperature using "Front-Face" and "Rear-Face" Laser Flash Methods

B. Hay · J.-R. Filtz · J. Hameury · G. Davée · L. Rongione · O. Enouf

Received: 11 October 2008 / Accepted: 12 January 2009 / Published online: 31 January 2009

Abstract Thick ceramic coatings deposited by plasma spraying techniques are widely used as wear and corrosion resistant coatings at high temperature. To measure accurately the thermal diffusivity of such coatings, the diffusivimeter of LNE has been set up to allow multilayered material studies up to 1,400 °C by *rear-face* and *front-face* laser flash methods. These two methods have been compared in a large temperature range by measuring the thermal diffusivity of homogeneous (Armco iron and Poco graphite) and multilayered materials (chromium oxide coating deposited on iron alloy substrate). The thermal-diffusivity values measured by using *front-face* and *rear-face* techniques are in good agreement, with a relative deviation of less than 5 % depending on temperature and materials.

Keywords Ceramic coating · Chromium oxide · High temperature · Laser flash method · Pulsed photothermal radiometry · Thermal diffusivity

1 Introduction

Specific coatings are often deposited on materials for protection purposes or for improving optical or surface mechanical properties (e.g., hardening). A critical case concerns thermal barrier coatings, typically zirconia deposited on a metallic substrate, used in the aircraft and automotive industries as heat and wear shields of engine components. As these ceramic layers are likely to evolve when operating at high temperature (e.g., by sintering), it is needed to estimate their thermophysical prop-

B. Hay (✉) · J.-R. Filtz · J. Hameury · G. Davée · L. Rongione · O. Enouf
Thermophysical Properties Laboratory, Thermal and Optical Division,
Laboratoire National de Métrologie et d'Essais, 1 rue Gaston Boissier,
75015 Paris, France
e-mail: bruno.hay@lne.fr

erties under their usage conditions in order to predict their thermal behavior. The morphology of a coating layer, and therefore its density and thermal conductivity, depend on the coating process. It is thus rarely possible to estimate the thermophysical properties of a coating from those of the bulk material. To avoid a destructive delamination of the coating from the substrate leading to modifications of the structure, thermal property measurements have to be undertaken directly on the multilayer composite.

LNE has performed for many years thermal-diffusivity measurements of homogeneous materials up to 1,400 °C in argon or vacuum environments by using a setup based on the traditional principle of the *rear-face* laser flash method [1,2]. A cylindrical specimen is irradiated on its front face by a short laser pulse, and the induced transient temperature rise on its rear face is measured as a function of time. In the case of a bulk homogeneous material, the thermal diffusivity is estimated according to the "partial time moments method" [3]. This estimation method, which was notably used by LNE in the certification process of Pyroceram 9606 as BCR-724 reference material [4], is not convenient for the study of coatings or multilayered materials.

An estimation procedure allowing thermal-diffusivity measurements of coatings by *rear-face* and *front-face* laser flash methods with the LNE setup has been proposed by Krapez et al. [5]. It is based on minimizing the difference between the experimental temperature–time curve (thermogram) and the corresponding theoretical values obtained by modeling the transient heat conduction through a multilayered system. The heat conduction equation is analytically solved in Laplace space by the quadrupole method [6]. A Stehfest algorithm [7] for the numerical inversion of Laplace transforms is applied to the results in order to obtain the transient temperature of the rear or front specimen sides. The estimation of the thermal diffusivity of the coating is performed using a least-squares method, with the thermophysical properties of the substrate being known. A sensitivity study of the used theoretical model has been done in order to define the limits of the temporal domain of analysis leading to the best results in terms of reliability and uncertainty of the estimated parameters (thermal diffusivity and heat losses) [5]. It shows notably that for the *rear-face* flash method, the thermal-diffusivity measurement accuracy decreases when the thickness of the substrate increases, due to the delay and attenuation of the thermal output signal naturally introduced by the substrate. The pulsed photothermal radiometry technique or *front-face* flash method appears as a good alternative solution. It consists of determining the thermal diffusivity from the temperature decay of the specimen front face. Provided that there is a significant difference between the thermal properties of the coating and of the substrate, this method can allow simultaneous measurements of the thermal diffusivity and thermal effusivity of a coating, whatever may be the substrate thickness.

LNE's reference bench has been set up to allow accurate thermal-diffusivity measurements of coatings up to 1,400 °C by *rear-face* and *front-face* laser flash methods. Both methods have been cross-checked by measuring the thermal diffusivity of, successively, well-known homogeneous materials (Armco iron and Poco graphite) and Cr_2O_3 coating deposited on an iron substrate from room temperature up to 1,400 °C. This article describes the design of the setup, the measurement methods implemented, as well as the results obtained on homogeneous and multilayered materials.

2 Description of the Setup

The current reference diffusivimeter of LNE is mainly composed of three parts concerning: the heating of the specimen at an isothermal temperature, the transient excitation of its front face, and the thermal response measurement on its rear face.

2.1 Description of the Laser Flash Diffusivimeter

A schematic view of the measurement arrangement is shown in Fig. 1. The short thermal excitation (around 450 µs) is generated by a Nd:phosphate glass laser of 1,054-nm wavelength. The laser beam is directed by a flat dielectric mirror M_1 to a resistive furnace allowing heating of the tested specimen (10 mm in diameter and about 1–5-mm thick) from room temperature to 1,400 °C. The furnace is a vertical cylinder closed at both ends by two ZnSe windows, which are transparent to the laser wavelength and to the working wavelength range of the used IR detectors.

The steady-state temperature of the specimen is measured by a Type S thermocouple, situated close to it. A photodiode is used to determine the duration, the form of the pulse, and the time origin that corresponds to the time when the laser beam irradiates the specimen.

The transient temperature rise on its rear face is measured by optical means with two IR detectors (HgCdTe or InSb depending on the temperature). The parabolic mir-

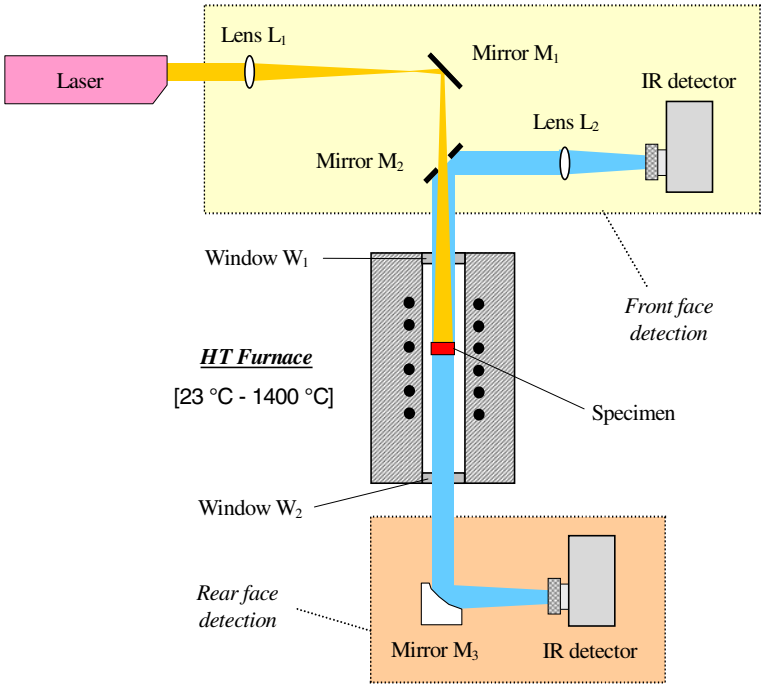

Fig. 1 Schematic view of the measurement setup

ror M_3 coated with gold is used to collect the emitted infrared radiation and focus it on the IR detectors.

A specific amplification system is associated with each detector in order to optimize the signal-to-noise ratio. The analog signal delivered by the detector is first amplified, with a resistance bridge device or a current/voltage converter, depending on the type of detector (photoconductor or photovoltaic). The baseline (constant signal before the pulse) is then subtracted using a differential amplifier. The signal is finally filtered by a low-pass filter having a cut-off frequency of 30 kHz, before being converted by the A/D converter of an NI PCI-6052 data acquisition device. All the parameters of the data acquisition (amplification gains, frequency, number of acquisition points, amount of pre-trigger, etc.) are chosen by the user from a Labview human–machine interface. The beginning of the data acquisition is synchronized with the laser flash using a trigger signal generated by the NI PCI-6052 data acquisition device. The signals coming from the IR detectors prior to the trigger (corresponding to the baseline of the thermogram) are stored continuously in a circular pre-trigger memory. When the trigger is detected, the new data are stored in a post-trigger memory.

2.2 Design of the *Front-Face* Optical System

A new "front-face detection" system has been recently fitted to the existing setup in order to measure the temperature evolution of the front face at the location of the thermal disturbance. The laser beam, which has an initial diameter of around 12 mm, is focused by the BK7 lens L_1 (see Fig. 1) some millimeters before the 90° flat mirror M_1, and passes through a hole (5-mm diameter) situated in the center of mirror M_2. It diverges in the furnace to irradiate the whole front face of the specimen. The IR radiation emitted by the specimen is directed by the flat mirror M_2 to the IR detector. It is focused by ZnSe lens L_2 on the sensitive element of the IR detector (1 mm diameter). Thus, the zone viewed from the detector is the image of the sensitive element on the specimen. The alignments of the optical elements (lenses, mirrors, etc.) are performed with a HeNe laser concentric with the Nd:phosphate glass laser.

Figure 2 shows the optical path of the laser beam taking into account the choice of the optical devices and of their positions. The propagation axis of the beam is represented by the *x*-axis. The *y*-axis represents the radius of the beam and the optical elements. The dotted line is the edge of the beam at $1/e^2$ (i.e., for a beam diameter containing 86.5 % of the total power in the case of a Gaussian beam) when it spreads without optics. The bold line represents the edge of the beam on the same path in the presence of optical devices; from left to right: convergent lens L_1, flat mirror M_1, flat mirror M_2 (with hole), window W_1, and specimen.

2.3 Theoretical Validation of the *Front-Face* Optical System by Optical Simulations

This optical configuration has been validated with optical simulations by a ray-tracing method. They show that by tilting the window W_1 a few degrees (4°) from the horizontal, the reflections of the laser beam, which could be possibly present on this window

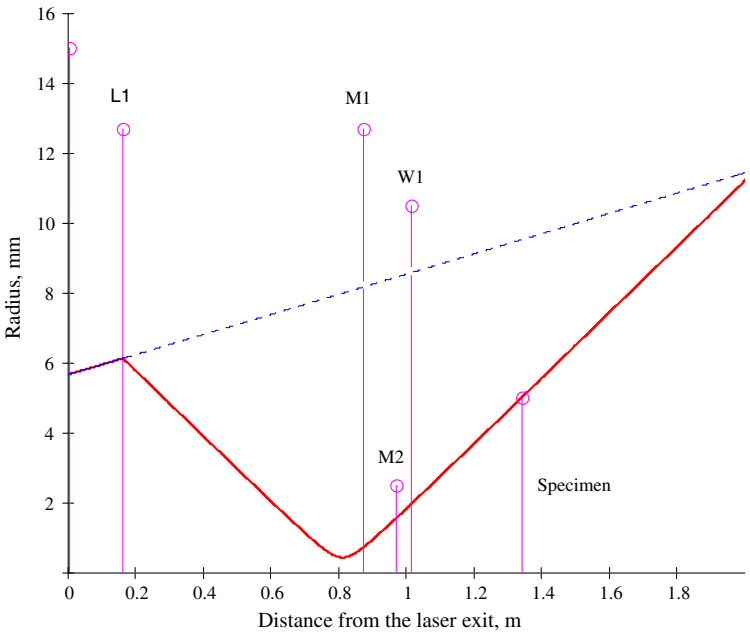

Fig. 2 Optical path and dimensions of the laser beam

despite its anti-reflection treatment, do not pass through lens L_2 and are therefore not focused on the detector. This reduces the risk to have a parasitic peak at the beginning of the thermogram and to damage the detector. Moreover, the IR radiation emitted by the specimen is overwhelmingly focused on the sensitive element of the IR detector; only a small portion passes through the hole of the mirror M_2.

These simulations have also allowed acquisition of some illumination maps in the plane of the detector and the specimen, by considering that it behaves like a black-body at 1,000 K on the spectral bandwidth from 2 µm to 12 µm. They show that the laser irradiates the entire surface of the specimen (see Fig. 3a) and that the image of the specimen by optical lens L_2 has a diameter of 1 mm in the plane of the sensitive element of the IR detector equivalent to this one (see Fig. 3b).

3 Validation of the Method

3.1 Application to the Case of Homogeneous Materials

The validation of the *front-face* flash method has been accomplished by measuring the thermal diffusivity of two well-known homogeneous materials: Armco iron and Poco AXM-5Q1 graphite. Figures 4 and 5 present examples of experimental thermograms (ln/ln scales) obtained at 400 °C, respectively, on the rear- and front faces of an Armco iron specimen.

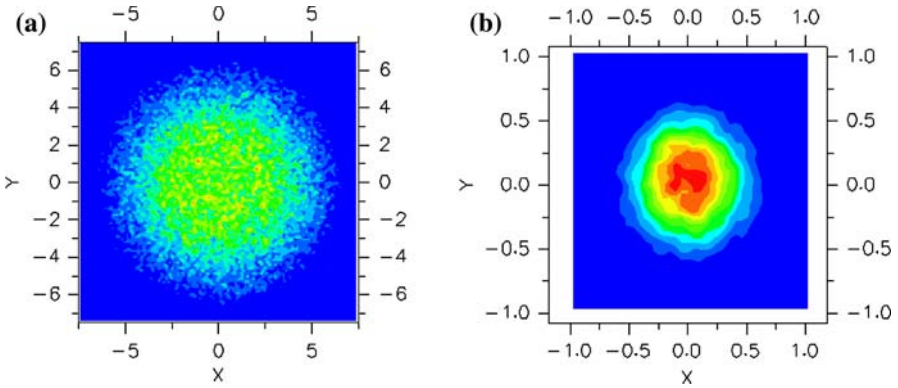

Fig. 3 Illumination maps in the plane of the specimen and of the IR detector. (**a**) Laser impact on the specimen. (**b**) Radiation emitted by the specimen on the detector

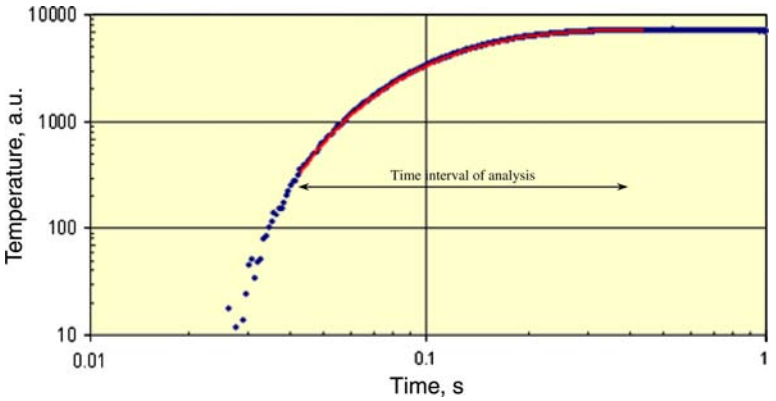

Fig. 4 Thermogram obtained at 400 °C on the rear face of an Armco iron specimen

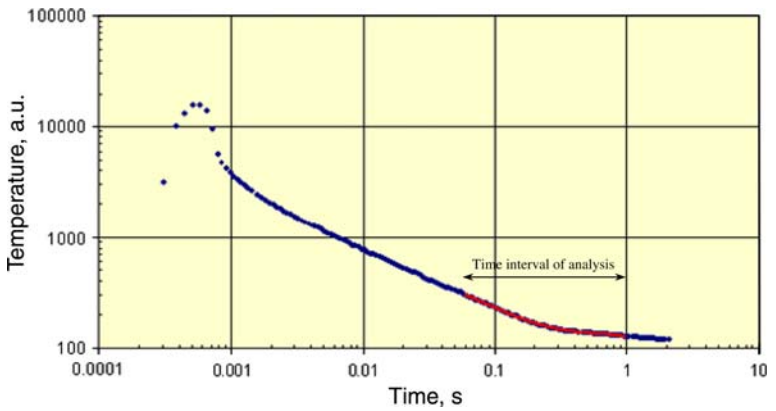

Fig. 5 Thermogram obtained at 400 °C on the front face of an Armco iron specimen

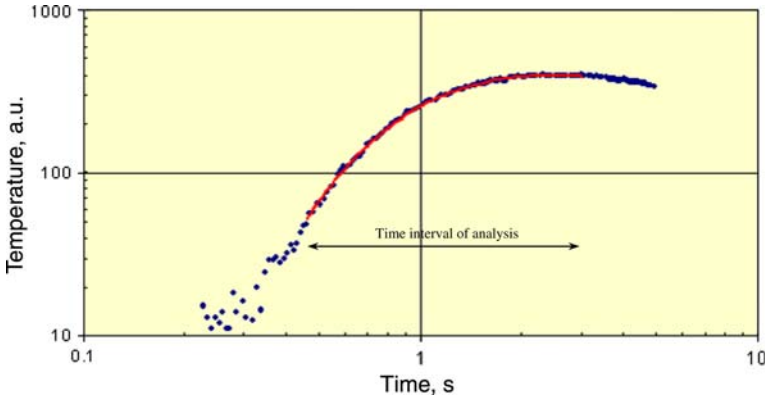

Fig. 6 Thermogram obtained at 600 °C on the rear face of a multilayer Cr_20_3/Fe

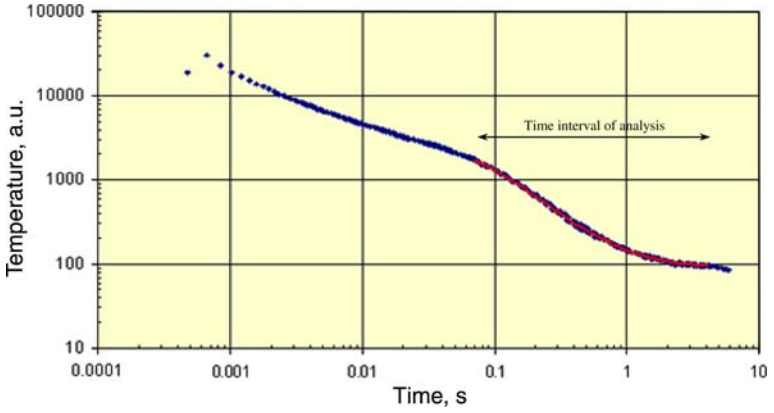

Fig. 7 Thermogram obtained at 600 °C on the front face of a multilayer Cr_20_3/Fe

The time interval of analysis on which the parameter estimation was performed according to [5] is represented in Figs. 4, 5, 6, and 7 by a double arrow. Figure 4 shows a "classical" shape of a rear-face thermogram, where the maximum signal is reached around 0.5 s after the energy deposit and is followed by a very small decrease due to weak heat losses. The thermogram presented in Fig. 5 shows that the maximum signal, reached 0.6 ms after the energy deposit on the front face, is followed by a decrease with a slope in $t^{-1/2}$, characteristic of the thermal behavior of a semi-infinite medium. When the heat reached the specimen rear face, an "elbow" appears at 0.3 s and is followed by a quasi-adiabatic evolution. Actually, the temperature of the front face continues to decline due to heat losses on both sides. It is approximately the temporal location of this bend, which allows the identification of the thermal diffusivity of a homogeneous material. Accordingly, the time interval of analysis surrounds this bend on approximately from one decade of time to one decade and a half (see Figs. 4, 5, 6, and 7).

Table 1 Armco iron—comparison of "front-face" and "rear-face" measurements

Armco iron (Thickness = 2.802 mm at 23 °C)						
Temperature (°C)	Thermal diffusivity (10^{-6} m$^2 \cdot$ s^{-1})					
	Results from Refs. [9–13] ①	Rear face			Front face	
		Moment	Minimization	Rel. dev. ② (%)	Minimization	Rel. dev. ③ (%)
23	20.25	20.47	20.35	0.6	20.24	0.5
200	14.40	14.54	14.56	−0.1	14.47	0.6
400	9.93	10.02	10.04	−0.1	10.14	−1.0
600	6.57	6.56	6.51	0.7	6.47	0.7
800	4.48	4.47	4.41	1.4	4.45	−1.0

Table 2 Poco graphite—comparison of "front-face" and "rear-face" measurements

Poco AXM-5Q1 graphite (Thickness = 2.991 mm at 23 °C)						
Temperature (°C)	Thermal diffusivity (10^{-6} m$^2 \cdot$ s^{-1})					
	Results from Refs. [9–13] ①	Rear face			Front face	
		Moment	Minimization	Rel. dev. ② (%)	Minimization	Rel. dev. ③ (%)
23	81.22	78.76	75.91	3.7	76.22	−0.4
200	45.17	44.62	44.04	1.3	45.54	−3.3
400	29.42	28.62	28.61	0.0	29.25	−2.2
600	22.48	21.97	21.89	0.3	22.51	−2.8
800	18.08	17.87	17.87	0.0	18.05	−1.0
1000	15.19	15.06	14.82	1.6	15.28	−3.1
1200	13.55	13.35	13.29	0.5	13.30	−0.1
1400	12.22	12.24	12.04	1.7	12.34	−2.5

Tables 1 and 2 present the thermal-diffusivity results obtained on Armco iron and Poco AXM-5Q1 graphite specimens. These results are the average of three successive measurements performed under the same experimental conditions. The column indexed ① gives values coming from polynomial expressions, determined by LNE [2] from results reported by several authors [8–13]. The measurements carried out on the rear face have been analyzed using the two methods of identification described previously: the "partial time moments method" and a minimization method proposed by Krapez. The objective of this approach is to compare this last method with a well-tested method in the case of "well-known" materials. These two methods are, respectively, referenced *Moment* and *Minimization* in Tables 1 and 2. The column indexed ② gives the relative deviation between the results obtained by the two methods. In the case of measurements performed on the front face, only the method of minimization is used because the partial time moments method can not be applied to this configuration of

measurement. The column indexed ③ gives the relative deviation between the results obtained with the method of minimization on the front face and rear face.

The relative variations between all our measurements and the values resulting from the polynomial expressions are less than 2 % for Armco iron and less than 3 % for Poco AXM-5Q1 graphite (except at 23 °C where this relative variation is 6.5 %). The relative deviation (index ②) between the results obtained by the two methods of identification is less than 2 % (except for graphite at 23 °C) over the temperature range from 23 °C to 1,400 °C for the two homogeneous materials. It can be considered that these two methods lead to identical results, the relative expanded uncertainty ($k = 2$) on thermal-diffusivity measurements of Armco iron and Poco graphite by the partial time moments method being estimated between ±3 % and ±5.5 % over the temperature range from 23 °C to 1,400 °C [14,15]. The results of measurements also show good consistency with a relative deviation (index ③) of less than 3.5 % between the values obtained by the front-face and rear-face methods. The repeatability of three measurements is better than 1.5 % up to 1,400 °C for rear-face measurements, and less than 2 % below 800 °C, and better than 3 % for temperatures between 800 °C and 1,400 °C for front-face measurements.

3.2 Application to the Case of Multilayer Materials

After having validated the front-face flash method in the case of homogeneous materials, both front-face and rear-face methods have been applied to the case of multilayer materials, constituted by a chromium oxide coating deposited by plasma spraying on an iron alloy substrate. These kinds of thick ceramic coatings are notably applied to engine components such as a piston crown, exhaust valves, and cylinder liner. Chromium oxide coatings are very resistant to wear [16], to abrasion in aggressive environment, and to high temperature corrosion. Measurements have been performed between 23 °C and 800 °C on the two following coating/substrate systems:

A. 0.229 mm of Cr_2O_3 coating on Fe substrate of 0.997 mm thick,
B. 0.405 mm of Cr_2O_3 coating on Fe substrate of 6.000 mm thick.

The thermal properties of the substrate must be known to enable thermal-diffusivity characterization of the coating. The thermal expansion, density, specific heat, and thermal diffusivity of the substrate have therefore been previously measured from 23 °C to 800 °C by LNE on naked specimens, respectively, by push-rod dilatometry, the immersion method, differential scanning calorimetry, and the rear-face laser flash method. The obtained results are presented in Table 3.

Figures 6 and 7 give examples of experimental thermograms (ln/ln scales) obtained at 600 °C, respectively, on the rear and front faces of the coating/substrate system B. The rear-face thermogram, shown in Fig. 6, has a quite similar appearance to that of a homogeneous material (see Fig. 4), with no visible distinctive feature in relation with the heterogeneity of the thermal properties of the multilayer. Conversely, the front-face thermograms clearly differ for a homogeneous material and a multilayer one.

Figure 7 shows, as in the case of homogeneous materials (see Fig. 5), that the temperature initially follows a decrease in slope in $t^{-1/2}$, as if the coating was alone. But after a first elbow situated near 0.1 s (corresponding to the time when the heat

Table 3 Thermal properties of the iron alloy substrate

Temperature (°C)	a (10^{-6} m$^2 \cdot$ s^{-1})	α (10^{-6} K^{-1})	ρ (kg $\cdot$ m^{-3})	c_p (J $\cdot$ kg$^{-1} \cdot$ K^{-1})
23	16.53	–	7814	463
200	13.22	14.1	7756	517
400	9.72	14.5	7687	585
600	6.46	15.0	7614	696
800	4.47	15.4	7540	798

Table 4 Multilayer Cr_2O_3/Fe—comparison of "front-face" and "rear-face" measurements

Cr_2O_3 Coating						
Temperature (°C)	Thermal diffusivity (10^{-6} m$^2 \cdot$ s^{-1})					
	Multilayer A			Multilayer B		
	Rear face	Front face	Rel. dev. (%)	Rear face	Front face	Rel. dev. (%)
23	1.283	1.292	−0.7	1.325	1.260	5.0
200	1.084	1.100	−1.5	0.992	0.954	3.9
400	0.877	0.895	−2.0	0.756	0.779	−3.1
600	0.856	0.877	−2.4	0.773	0.782	−1.1
800	0.840	0.860	−2.4	0.831	0.809	2.7
23	1.635	1.672	−2.3	1.373	1.319	4.0

reaches the substrate), the decrease accelerates up to a second elbow located around 1 s. After this elbow, which represents the time when the heat reaches the rear face of the multilayer, the temperature approaches to the adiabatic stage corresponding to the case of the multilayer without losses. As previously, the multilayer being subjected to heat losses, the temperature of the front face continues to actually decline. The thermal diffusivity of the coating is identified by the temporal location of this transition zone.

Table 4 presents a comparison of thermal-diffusivity results measured on the front face and rear face on both configurations of Cr_2O_3/Fe multilayers. The thermal diffusivity values obtained are in a good agreement with those given in the literature [16,17]. The relative deviation between the results obtained by the two methods is a maximum of 5 % over the temperature range from 23 °C to 800 °C for both multilayers. However, this deviation is higher for multilayer B (Cr_2O_3/Fe of 0.405 mm/6.000 mm) than for multilayer A (Cr_2O_3/Fe of 0.229 mm/0.997 mm). The repeatability of three consecutive measurements is better than 2 % for the measurements carried out on the front face of the two multilayers, and on the rear face of multilayer A. It grows up to 7 % for measurements performed on the rear face of multilayer B. These observations can be explained by a higher damping of the thermal signal for the thicker multilayer than for the thinner one. This leads inevitably to a worse signal-to-noise ratio of rear-face measurements for multilayer B than for multilayer A. These results corroborate the conclusions of the sensitivity study [5] presented in the introduction.

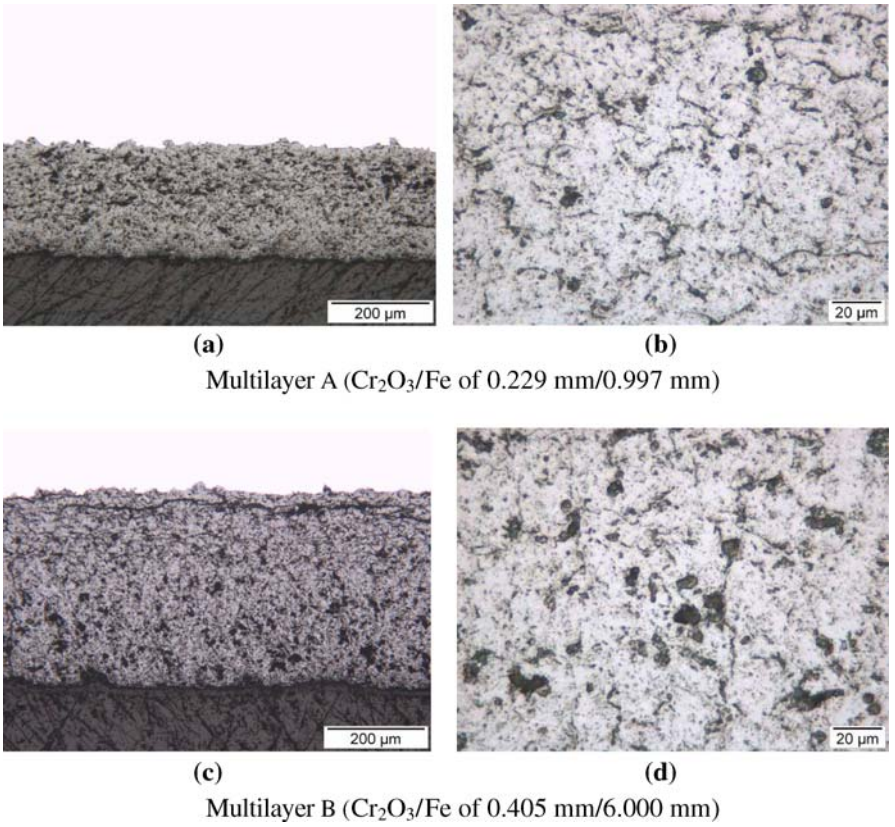

Fig. 8 Cross-sectional microstructures of the chromium oxide coatings. Multilayer A (Cr_2O_3/Fe of 0.229 mm/0.997 mm) (**a**) 100× magnification, (**b**) 500× magnification. Multilayer B (Cr_2O_3/Fe of 0.405 mm/6.000 mm) (**c**) 100× magnification, (**d**) 500× magnification

The results given in Table 4 highlight also a drift of the thermal diffusivity of chromium oxide with thermal cycling. The values acquired at 23 °C after thermal cycling are higher than those originally obtained (increase of nearly 30 % for multilayer A). This phenomenon is probably due to a modification of the ceramic by sintering. In addition, the values of thermal diffusivity obtained with multilayer A are a little higher than those determined with multilayer B. After performing the thermal-diffusivity measurements, the microstructures of both coatings have been investigated by optical microscopy in order to explain this behavior. A comprehensive imaging system, consisting of a high magnification optical microscope coupled to a CCD camera, was used. This system has been calibrated in length in order to measure the thickness of the coatings with an uncertainty of a few µm. The obtained images, presented in Fig. 8, show clearly that the aspect of the deposit is different depending on its thickness and that the thicker coating contains more pores and cracks than the thinner one (the substrates appearing in white on the microscope images).

Coatings applied by plasma spraying have a lamellar microstructure and often present several types of defects (nonhomogenous phase structure, open porosity, cracks, etc.) linked to the processing technique [18,19]. These cracks, resulting from the relaxation of the residual stresses during thermal cycling, are all the more numerous since the coating is thick [20]. The slight difference of the coatings' microstructure could thus explain the difference between the thermal diffusivity values obtained for both coatings.

4 Conclusion

LNE has upgraded its reference diffusivimeter in order to measure the thermal diffusivity of ceramic coatings at high temperature using *front-face* and *rear-face* laser flash methods. The two methods have been first compared on homogeneous materials (Armco iron and Poco AXM-5Q1 graphite) from room temperature up to 1,400 °C. This comparison phase clearly indicated that *front-face* and *rear-face* methods led to identical results, the obtained values differing by less than 3.5 % (with a relative expanded uncertainty less than 5.5 %). Thermal diffusivities of ceramic coatings have been then measured on multilayer materials (chromium oxide coating deposited on iron alloy substrate). The thermal-diffusivity values measured according to the two methods are in good agreement, with a relative deviation of less than 5 % depending on temperature and materials. The obtained experimental results show that it is better to determine the thermal diffusivity of a homogeneous material by applying the *rear-face* flash method, and of a coating by using the *front-face* flash method, especially when the substrate is thick. The next step will be to estimate simultaneously the thermal diffusivity and thermal effusivity of a ceramic coating by applying the *front-face* laser flash method.

Acknowledgment The authors wish to thank Dr. J.C. Krapez from ONERA for developing the used parameters estimation procedure.

References

1. W.J. Parker, R.J. Jenkins, C.P. Bulter, G.L. Abbott, J. Appl. Phys. **32**, 1679 (1961)
2. B. Hay, J.-R. Filtz, J.-C. Batsale, *Mesure de la diffusivité thermique par la méthode flash* (Techniques de l'Ingénieur, R2955, 2004)
3. A. Degiovanni, M. Laurent, Rev. Phys. Appl. **21**, 229 (1986)
4. B. Hay, L. Rongione, J.-R. Filtz, J. Hameury, High Temp.-High Press. **37**, 13 (2008)
5. J.C. Krapez, B. Hay, D. Demange, G. Gardette, P. Levesque, F. Passilly, *Méthode flash en face avant. Optimisation de l'expérience pour un monocouche et un bicouche* (Congrès SFT, Vittel, 2002)
6. D. Maillet, S. André, J.C. Batsale, A. Degiovanni, C. Moyne, *Thermal Quadrupoles. Solving the Heat Equation Through Integral Transforms* (Wiley, New York, 2000)
7. H. Stehfest, Commun. ACM. **13**, 47 (1970)
8. Y.S. Touloukian, R.W. Powell, C.Y. Ho, M.C. Nicolaou, *Thermophysical Properties of Matter. Thermal Diffusivity*, vol. 10 (IFI/Plenum, New York, 1973)
9. H.R. Shanks, A.H. Klein, G.C. Danielson, J. Appl. Phys. **38**, 2885 (1967)
10. L. Filoni, L. Lorenzoni, High Temp.-High Press. **23**, 309 (1991)
11. A. Dobrosavljevic, N. Perovic, K. Maglic, High Temp.-High Press. **19**, 303 (1987)

12. J.G. Hust, *A Fine-Grained Isotropic Graphite for Use as NBS Thermophysical Property RM's from 5 to 2500 K* (NBS Special Publication, 1984), pp. 260–289
13. T. Baba, A. Cezairliyan, Int. J. Thermophys. **15**, 343 (1994)
14. B. Hay, J.-R. Filtz, J. Hameury, L. Rongione, Int. J. Thermophys. **26**, 1883 (2005)
15. B. Hay, J.-R. Filtz, J. Hameury, L. Rongione, Rev. Française Métrologie **14**, 3 (2008)
16. C. Ding, Z. Tong, D. Yan, in *Plasma Spraying-Theory and Applications*, ed. by R. Suryanarayanan (World Scientific Pub. Co., Singapore, 1993), pp. 163–178
17. L. Pawlowski, P. Fauchais, Int. Mater. Rev. **37**, 271 (1992)
18. C. Ding, B. Huang, H. Lin, Thin Solid Films **118**, 485 (1984)
19. M. Vippola, P. Vuoristo, T. Lepistö, T. Mäntylä, J. Mater. Sci. Lett. **22**, 463 (2003)
20. T. Mäntylä, *Thick Ceramic Coatings*, Euroceram news 7, available via http://www.euroceram.org/en/news/news7.pdf. Accessed 5 June 2007 (2002)